



Crystal structure and electronic properties of two nimesulide derivatives: A combined X-ray powder diffraction and quantum mechanical study

Abir Bhattacharya^a, Soumen Ghosh^a, Kavitha Kankanala^{b,c}, Vangala Ranga Reddy^d, Khagga Mukkanti^b, Sarbani Pal^c, Alok K. Mukherjee^{a,*}

^a Department of Physics, Jadavpur University, Jadavpur, Kolkata 700032, India

^b JNT University, Kukatpally, Hyderabad 500072, India

^c Department of Chemistry, PG Campus, MNR Degree and PG College, Kukatpally, Hyderabad 500085, India

^d Dr. Reddy's Laboratories Ltd., Integrated Product Development Bachupally, Hyderabad 500055, India

ARTICLE INFO

Article history:

Received 27 January 2010

In final form 7 May 2010

Available online 13 May 2010

ABSTRACT

Crystal structures of two nimesulide derivatives, C₁₃H₁₄O₃N₂S (**2**) and C₂₁H₁₆O₅N₂S (**3**), have been determined from X-ray powder diffraction data and their electronic structures were calculated at the DFT level. The optimized molecular geometries of **2** and **3** correspond closely to that obtained from the crystallographic analysis. Intermolecular hydrogen bonds and $\pi \dots \pi$ stacking interactions form supramolecular assembly in both compounds. The HOMO–LUMO energy gap (>2.2 eV) indicates a high kinetic stability of both compounds. Although the compound **2** does not exhibit any anti-inflammatory activity, **3** can induce 34% edema inhibition in rat paws.

© 2010 Elsevier B.V. All rights reserved.

1. Introduction

Nimesulide, N-(4-nitro-2-phenoxyphenyl) methanesulfonamide (**1**), is an effective non-steroidal anti-inflammatory drug (NSAID), which can inhibit cyclooxygenase-2 (COX-2) enzyme selectively [1]. The selective inhibition of COX-2 is attributed mainly to the presence of methanesulfonamide group, and the overall molecular conformation of **1** which facilitates strong interactions with the enzyme [2]. In addition to good anti-inflammatory, analgesic, anti-pyretic activities and low gastrointestinal toxicity, **1** is also useful in a wide range of disorders, which include various arthritic conditions, gynaecological and urological problems, post-surgical and cancer pain, and vascular diseases [3]. Several analogues of nimesulide (**1**) aimed at enhancing the anti-inflammatory activity and reducing its toxicity have been reported by changing in **1** the R-group of the –NHSO₂R moiety, the electron withdrawing group at the C-4 position and the central aryl ring by a pyridine or pyridinium moiety [4–6]. The X-ray structure analyses and molecular dynamics simulations of COX-2 complexes with nimesulide analogues indicate a network of hydrogen bonds in the COX-2 active site involving the nitrogen and oxygen atoms of the inhibitor molecule [7,8]. Thus knowledge of crystal structures of nimesulide derivatives is of key importance for a better understanding of their structure–activity relation.

In general, single-crystal X-ray diffractometry is the method of choice when it comes to crystal structure determination; although

for many materials it can be difficult to grow single crystals of appropriate size and quality that make them amenable to structure analysis. In such cases, structure determination using X-ray powder diffraction data may be the only viable option for structural characterization. With the recent developments of the direct-space strategy for structure solution [9–12], *ab initio* crystal structure analysis of organic molecular solids can now be accomplished from X-ray powder diffraction data. Crystal structures of several molecular compounds have been determined from laboratory X-ray powder data using the direct-space approaches [13–15].

The present Letter reports the synthesis and structural characterization of two nimesulide derivatives, N-(4-amino-2-phenoxyphenyl) methanesulfonamide (**2**) and N-[4-(1,3-dioxo-1,3-dihydroisindol-2-yl)-2-phenoxyphenyl] methanesulfonamide (**3**), along with the DFT calculations to investigate the molecular geometry and the electronic structure. To the best of our knowledge, this is the first example of structure determination of nimesulide analogues from X-ray powder diffraction data.

2. Materials and methods

2.1. Synthesis

N-(4-amino-2-phenoxyphenyl) methanesulfonamide (**2**) was synthesized by catalytic hydrogenation of a magnetically stirred solution of nimesulide **1** (9 g, 28.1 mmol) in dry ethyl acetate (50 mL) using 5% Pd–C. The reaction was carried out at room temperature (27 °C) for 3 h. After completion of the reaction, as indicated by the thin layer chromatography (TLC), the solution was

* Corresponding author. Fax: +91 33 24146484.

E-mail address: akm_ju@rediffmail.com (A.K. Mukherjee).

filtered and the filtrate was concentrated under reduced pressure to obtain **2** (a reduced form of nimesulide **1**) in quantitative yield. The crude product was purified by recrystallization from methanol and chloroform mixture to afford light brown coloured microcrystalline powder of N-(4-amino-2-phenoxyphenyl) methanesulfonamide (**2**). Mp 198(2) °C. Elemental analysis: found C 56.25, H 5.07, N 10.26%; calculated for $C_{13}H_{14}N_2O_3S$: C 56.10, H 5.07, N 10.06%.

The cyclic amide, N-[4-(1,3-dioxo-1,3-dihydroisoindol-2-yl)-2-phenoxyphenyl] methanesulfonamide (**3**), was synthesized as follows. Anhydrous sodium acetate (100 mg) was added to a mixture of compound **2** (278 mg, 1.0 mmol) and phthalic anhydride (1.0 mmol) in glacial acetic acid (3 mL) and the mixture was allowed to reflux for 10 min. After completion of the reaction, the mixture was poured into crushed ice (50 g) and stirred. The solid separated was filtered and dried. The crude product on purification by column chromatography and crystallization from methanol yielded micro-

crystalline powder of N-[4-(1,3-dioxo-1,3-dihydroisoindol-2-yl)-2-phenoxyphenyl] methanesulfonamide (**3**) (yield 70%).

Microwave assisted method: a mixture of compound **2** (278 mg, 1.0 mmol), phthalic anhydride (1.0 mmol) and sodium acetate (100 mg) was exposed to microwave irradiation in a domestic microwave oven operating at 2450 MHz. After completion of reaction, the mixture was diluted with cold water (50 mL), stirred vigorously, filtered and dried to obtain the desired product **3** (yield 73%). Mp 231(2) °C. Elemental analysis: found C 61.70, H 3.94, N 6.89%, calculated for $C_{21}H_{16}N_2O_5S$: C 61.75, H 3.5, N 6.86%.

Elemental analyses (C, H, N) were performed using a Perkin-Elmer 240 C analyzer.

2.2. X-ray structure analysis

X-ray powder diffraction data were recorded at ambient temperature on a Bruker D8 Advance diffractometer operating in the

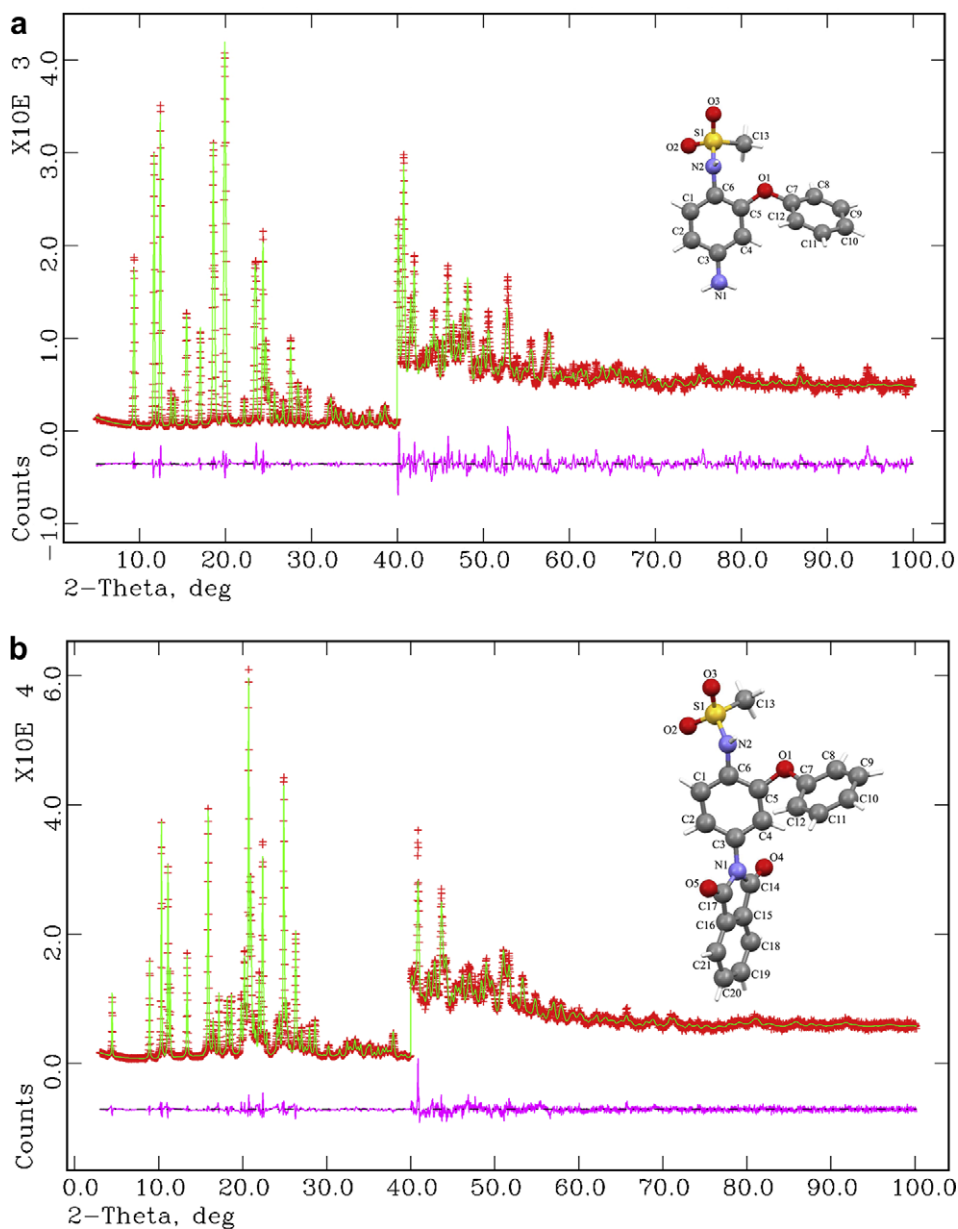


Fig. 1. Final Rietveld plots and molecular views of (a) $C_{13}H_{14}O_3N_2S$ (**2**) and (b) $C_{21}H_{16}O_5N_2S$ (**3**) with atom numbering scheme. Red crosses: observed pattern, green curve: calculated pattern, pink curve: difference curve. The vertical scale of the 40–100° (2θ) portion of the profiles has been multiplied by a factor of 10. (For interpretation of the references in colour in this figure legend, the reader is referred to the web version of this article.)

reflection mode and using $\text{CuK}\alpha_1$ radiation ($\lambda = 1.5406 \text{ \AA}$) selected with a germanium (1 1 1) incident-beam monochromator for **2**, and $\text{CuK}\alpha_2$ radiation ($\lambda = 1.5418 \text{ \AA}$) for **3**. The indexing of X-ray powder pattern of **2** using the program NTREOR [16] indicated a monoclinic unit cell with $a = 14.423(3)$, $b = 12.514(4)$, $c = 7.661(5) \text{ \AA}$ and $\beta = 100.11(1)^\circ$ [$M(20) = 17$, $F(20) = 35$ (0.011 605, 50)]. In **3**, the indexing result showed a triclinic unit cell with $a = 8.643(4)$, $b = 19.910(2)$, $c = 5.616(4) \text{ \AA}$, $\alpha = 90.40(3)$, $\beta = 95.62(1)$ and $\gamma = 91.81(2)^\circ$ [$M(20) = 38$, $F(20) = 75$ (0.012 955, 89)]. Statistical analysis of powder patterns using the EXPO 2004 [17] indicated the most probable space group as $P2_1/a$ for **2**, and $P\bar{1}$ for **3**, which were used for structure solution. The full pattern decomposition was performed in each case with EXPO 2004 following the Le Bail algorithm and using a Pearson VII peak profile function [18]. Good quality Le Bail fits, $R_p = 0.085$ in **2** and $R_p = 0.065$ in **3**, indicated the correctness of unit cells and the estimates of profile parameters for subsequent structure solution. The structures of **2** and **3** were solved by global optimization of structural models in direct-space based on a Monte Carlo search using the simulated annealing technique [19] (in parallel tempering mode), as implemented in the

Table 1
Crystal data and structure refinement parameters of $\text{C}_{13}\text{H}_{14}\text{O}_3\text{N}_2\text{S}$ (**2**) and $\text{C}_{21}\text{H}_{16}\text{O}_5\text{N}_2\text{S}$ (**3**).

Compound	$\text{C}_{13}\text{H}_{14}\text{O}_3\text{N}_2\text{S}$ (2)	$\text{C}_{21}\text{H}_{16}\text{O}_5\text{N}_2\text{S}$ (3)	$\text{C}_{13}\text{H}_{12}\text{O}_5\text{N}_2\text{S}$ (1) ^a
Formula weight	278.33	408.43	308.31
Temperature (K)	293(2)	293(2)	293(2)
Crystal system	Monoclinic	Triclinic	Monoclinic
Wavelength (\AA)	1.5406	1.5418	1.5418
Space group	$P 2_1/a$	$P\bar{1}$	$C 2/c$
a (\AA)	14.427(1)	8.659(3)	33.657(3)
b (\AA)	12.521(1)	19.949(8)	5.131(1)
c (\AA)	7.658(1)	5.629(2)	16.082(1)
α ($^\circ$)	90.0	90.40(1)	90.0
β ($^\circ$)	100.14(1)	95.64(1)	92.37(1)
γ ($^\circ$)	90.0	91.79(1)	90.0
Volume (\AA^3)	1361.8(3)	967.2(11)	2774.5(3)
Z	4	2	8
Density (calculated) g cm^{-3}	1.358	1.403	1.476
2θ interval ($^\circ$)	3–100	5–100	5–115
Step size ($^\circ$)	0.02	0.02	–
Counting time (s)	25	50	–
No. of variable parameters	181	123	194
No. of background points	10	10	–
R_p/R_1	0.0553	0.0464	0.0401
R_{wp}/wR	0.0758	0.0634	0.1146
R_F^2	0.1432	0.0498	–
χ^2/S	3.10	8.23	1.25

^a Structural data of $\text{C}_{13}\text{H}_{12}\text{O}_5\text{N}_2\text{S}$ (**1**) are taken from Dupont [29].

Table 2
Hydrogen bond geometries (\AA , $^\circ$) in $\text{C}_{13}\text{H}_{14}\text{O}_3\text{N}_2\text{S}$ (**2**) and $\text{C}_{21}\text{H}_{16}\text{O}_5\text{N}_2\text{S}$ (**3**).

D–H...A	$d(\text{D–H})$	$d(\text{H...A})$	$d(\text{D...A})$	$\angle(\text{DHA})$	Symmetry
<i>C</i> ₁₃ <i>H</i> ₁₄ <i>O</i> ₃ <i>N</i> ₂ <i>S</i> (2)					
N1–HN1A...O3	0.87	2.44	3.274(4)	161.7	$x + 1/2, -y + 1/2, z$
N1–HN1B...O2	0.87	2.42	3.179(4)	146.6	$-x + 1/2, y + 1/2, -z + 1$
N2–HN2...N1	0.88	2.34	2.923(6)	124.2	$-x + 1/2, y - 1/2, -z$
<i>C</i> ₂₁ <i>H</i> ₁₆ <i>O</i> ₅ <i>N</i> ₂ <i>S</i> (3)					
N2–HN2...O3	0.91	2.26	3.060(2)	146.8	$-x + 2, -y + 2, -z + 1$
C18–H18...O4	0.97	2.60	3.441(2)	145.1	$-x + 1, -y + 1, -z$
C21–H21...O5	0.97	2.54	3.324(2)	137.8	$-x + 2, -y + 1, -z + 2$
C13–H13B...O2	0.98	2.61	3.510(2)	152.4	$-x + 1, -y + 2, -z + 1$
C _g (4)–C _g (4)	–	–	4.576(8)	–	$-x + 1, -y + 1, -z + 1$
C _g (4)–C _g (4)	–	–	4.623(8)	–	$-x + 2, -y + 1, -z + 1$

C_g(4) is the centroid of the (C15/C16/C18–C21) phenyl ring.

program Fox [20]. The initial molecular geometry input in Fox was determined by the MOPAC 5.0 program [21].

The atomic coordinates obtained from Fox were used as the starting model for the Rietveld refinement using the GSAS program package [22] with an EXPGUI [23] interface. The lattice parameters, background coefficients and profile parameters were refined initially followed by the refinement of positional coordinates of all non-hydrogen atoms with soft constraints on bond lengths and bond angles, and planar restraints on the phenyl and isoindol-2-yl moieties. The background was described by the shifted Chebyshev function of first kind with 10 points regularly distributed over the entire 2θ range. A common isotropic displacement parameter has been refined for all non-hydrogen atoms in **2** and **3**. Hydrogen atoms were placed at the calculated positions with a fixed value of isotropic displacement parameter (0.08 \AA^2). In the final stage of refinement, preferred orientation correction was applied using the generalized spherical harmonic model. The powder sample of **2** was textured and the order of spherical harmonics necessary to describe the preferred orientation was 18 (texture index = 1.60). In **3**, however, spherical harmonics of order four was found to be adequate. The Rietveld refinement of **2** and **3** yielded good quality of fits (Fig. 1) with $R_p = 0.0553$, $R_{wp} = 0.0758$ and $R_F^2 = 0.1432$ for **2** and $R_p = 0.0464$, $R_{wp} = 0.0634$ and $R_F^2 = 0.0498$ for **3**. Relevant crystal data for **2** and **3** are summarized in Table 1.

2.3. Computational details

Density functional theory (DFT) calculations have been carried out in the solid state (periodic) for **2** and **3** with the DMOL³ code [24] in the framework of a generalized-gradient approximation (GGA) [25]. The geometry optimization was performed using the BLYP density functional [26,27] and a double numeric plus polarization (DNP) basis set. The atomic coordinates were taken from the final X-ray refinement cycle. Geometry optimizations were carried out without any structural constraints. The electronic structures were also calculated at the same level.

2.4. Anti-inflammatory property evaluation

Male adult albino Wister rats (100–200 g) were divided into separate groups of six animals each. The anti-inflammatory activity of compounds **2** and **3** was evaluated following the method described by Winter et al. [28]. The pedal inflammation in rat paws was induced by sub plantar injection of 0.1 ml carrageenan (0.2%) suspension in gum acacia into the right hind of rats. The rat paw thickness was measured with a vernier calipers before and 1 h after the carrageenan injection. The compounds **2** and **3** were injected (100 mg/kg) intraperitoneally to separate groups of

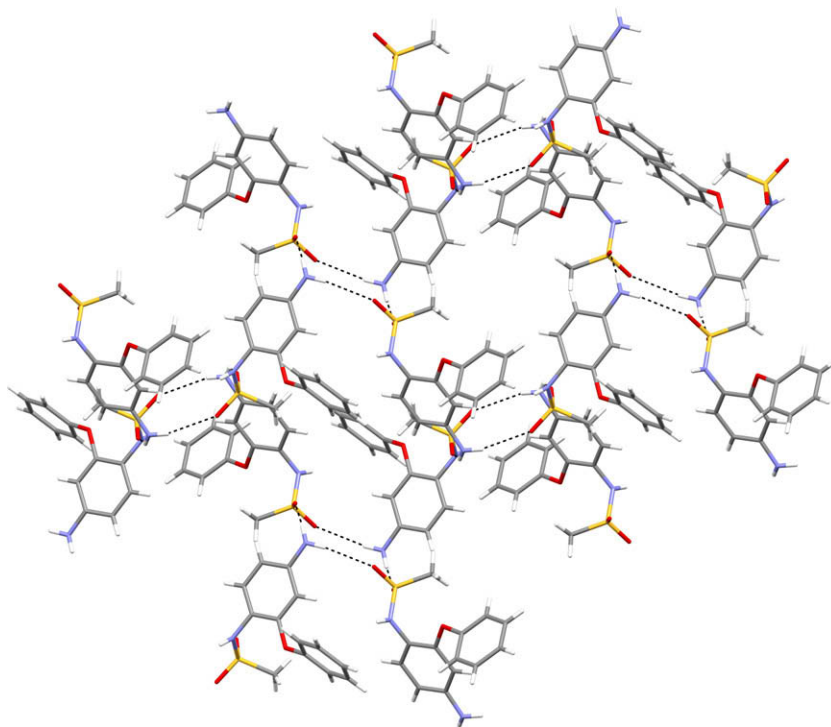


Fig. 2. Two-dimensional molecular assembly built with $R_4^4(12)$ and $R_4^4(36)$ rings in $C_{13}H_{14}O_3N_2S$ (**2**).

rats 1 h after the carrageenan injection. The control groups received the vehicle (5% gum acacia), while diclofenac sodium at a dose of 10 mg/kg was injected to the reference group. The difference between the thickness of two paws before and 1 h after the injection of the test compound (**2** or **3**) was taken as a measure of edema inhibition.

3. Results and discussion

3.1. Crystal and molecular structure

The molecular views of **2** and **3** with atom labeling scheme are shown in Fig. 1. The compounds **2** and **3** are the first structurally characterized nimesulide derivatives with substitution in the nitro group. The essential difference between the nimesulide (**1**) and the compounds **2** and **3** is that the nitro group in **1** is replaced by an amino group in **2** and dioxoisindol-2-yl moiety in **3**. The overall molecular conformation in **2** and **3** can be described in terms of dihedral angle between the oxygen-bridged phenyl rings, (C1–C6) and (C7–C12), of $66.4(2)^\circ$ in **2** and $65.8(6)^\circ$ in **3**, and the orientation of the methanesulfonamide group, which restricts any intramolecular C–H...O hydrogen bond. In the nimesulide (**1**) structure [29], the oxygen-bridged phenyl rings are inclined to each other by $74.69(8)^\circ$. The displacement of the oxygen atoms of the sulfonamide group prevents any hydrogen bond inside the COX-2 active site and consequently forms a less stable enzyme–ligand complex. Significant differences in the orientation of the methyl group with respect to the C6–N2 bond in the structures are established by the torsion angle C6–N2–S1–C13 of $-56.1(5)^\circ$ in **2** and $-78.0(9)^\circ$ in **3**. A comparison of C6–N2 [1.397(8)–1.419(6) Å] and N2–S1 [1.631(6)–1.658(7) Å] bond lengths in **2** and **3** (Supplementary Table 1) with that of nimesulide (**1**), 1.409(4) Å and 1.640(2) Å, where the sulfonamide group is not deprotonated, indicates that the compounds **2** and **3** are in the neutral form; the corresponding C6–N2 and N2–S1 distances in the zwitterionic form of nimesulide analogue are 1.354(2) Å and 1.609(1) Å, respectively [30]. For the –

NHSO₂CH₃ moiety, the sulfur–oxygen bond distances in **2** and **3** [1.427(7)–1.452(8) Å] are consistent with S=O distance and are similar to those found in related compounds [31–33]. These observations are supported by the DFT structure optimizations.

The crystal packing in **2** and **3** is stabilized by a combination of intermolecular N–H...O and C–H...O hydrogen bonds, and π ... π stacking interactions (Table 2). The supramolecular assembly in the compounds can be readily analyzed in terms of substructures of lower dimensionality with dimeric or tetrameric unit as the building block. Two pairs of intermolecular N–H...O hydrogen bonds in **2** (Table 2) with the amine N1 atom in the molecule at (x, y, z) acting as a double donor to the sulfonamide oxygen atoms O2 at $(1/2 - x, 1/2 + y, 1 - z)$ and O3 at $(1/2 + x, 1/2 - y, z)$ connect sets of four molecules into two types of rectangular motifs of inner core dimensions $4.5 \times 4.4 \text{ \AA}^2$ and $8.9 \times 10.5 \text{ \AA}^2$, respectively (Fig. 2). In terms of the graph set notation [34], these can be described as $R_4^4(12)$ and $R_4^4(36)$ rings. Adjacent $R_4^4(12)$ and $R_4^4(36)$ rings are edge fused to produce a two-dimensional supramolecular assembly in **2** (Fig. 2).

In **3**, a pair of intermolecular C–H...O hydrogen bonds (Table 2) between the centrosymmetrically related molecules involving the dioxoisindol-2-yl atoms, C18 at (x, y, z) and O4 at $(1 - x, 1 - y, -z)$, generates an $R_2^2(10)$ dimeric ring (M), Fig. 3, centered at $(1/2, 1/2, 0)$. Similarly, pairs of intermolecular C21–H21...O5 hydrogen bonds (Table 2) form another type of $R_2^2(10)$ ring (N), Fig. 3, centered at $(1, 1/2, 1)$. The two types of $R_2^2(10)$ rings are linked alternately to produce a C(13) chain [34] along the $[102]$ direction with a MNMN... sequence (Fig. 3). The parallel C(13) chains are joined through pairs of N2–HN2...O3 hydrogen bonds to form a rectangular two-dimensional grid of dimension $21.8 \times 10.7 \text{ \AA}^2$. The stacking of rectangular grids along the $[100]$ direction via π ... π interactions between the aryl rings of isindol-2-yl groups results into a three-dimensional supramolecular structure in **3**. Within the stack, the phenyl rings (C15/C16/C18–C21) of the molecules at (x, y, z) and $(1 - x, 1 - y, 1 - z)$, $(2 - x, 1 - y, 1 - z)$ are strictly parallel with interplanar spacings of 3.98 and 3.64 Å,

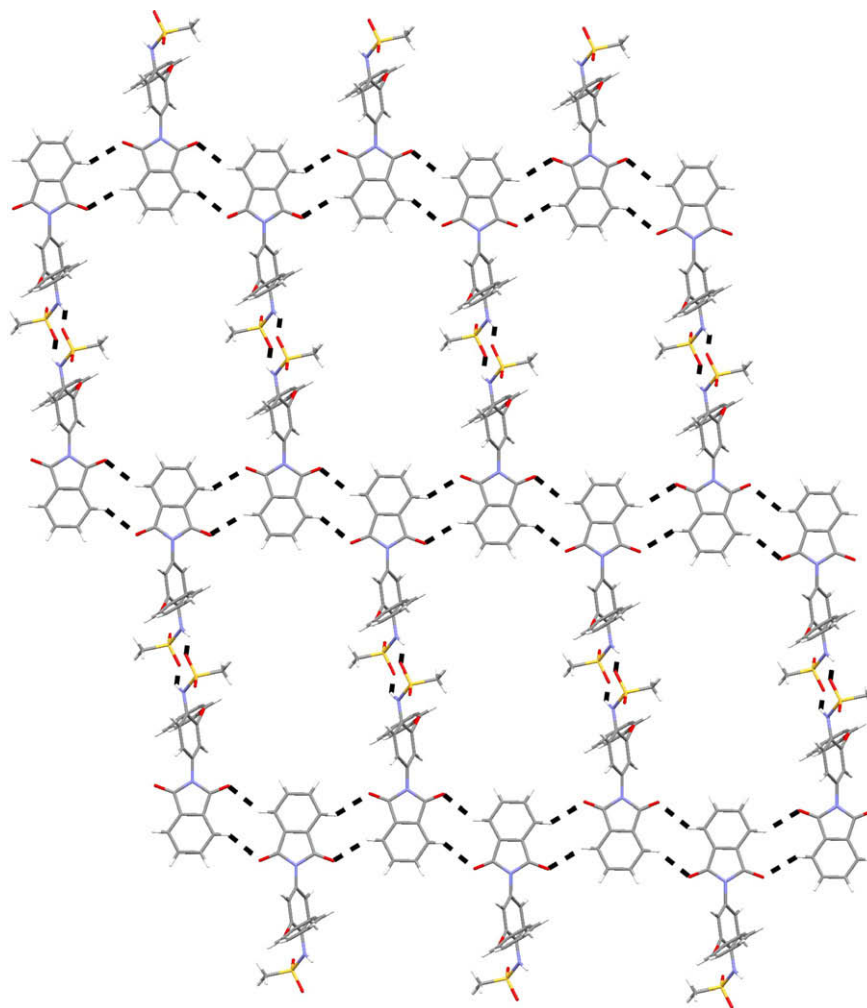


Fig. 3. A view of $R_2^2(10)$ rings and formation of two-dimensional grid in $C_{21}H_{16}O_5N_2S$ (**3**).

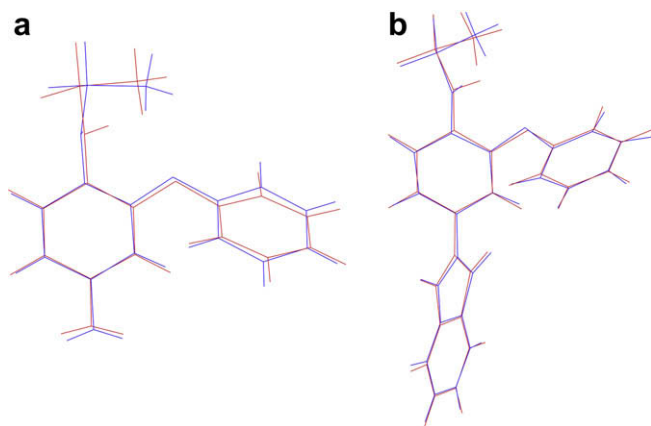


Fig. 4. Superposition of molecular conformation as obtained from X-ray structure analysis (blue) and solid state DFT calculation (red) for (a) $C_{13}H_{14}O_3N_2S$ (**2**) and (b) $C_{21}H_{16}O_5N_2S$ (**3**). (For interpretation of the references in colour in this figure legend, the reader is referred to the web version of this article.)

respectively; the corresponding ring offset and ring centroid separations are 2.27/4.576(8) Å and 2.85/4.623(8) Å, respectively. Hydrogen bond energies have been calculated for **2** and **3** as the energy difference, ΔE_{HB} , between the molecular packing with ($D \dots A < 3.5$ Å) and without hydrogen bond interaction ($D \dots A >$

3.5 Å). The evaluated ΔE_{HB} energies in **2** and **3** are 9.24 and 10.79 kcal mol⁻¹, respectively.

3.2. Electronic structure

The superposition of molecular geometries of **2** and **3** as established by the quantum mechanical calculations and the X-ray structure analyses shows excellent agreements (Fig. 4). Our DFT calculations concur that the observed molecular conformation is very close to that obtained via geometry optimization with regard to orientation of the methanesulfonamide group and also the twist of the phenyl ring (C7–C12) about the O1–C7 bond. The molecular energies of the X-ray analyzed and DFT calculated structures were –148.80 and –157.23 eV in **2**, and –221.89 and –230.04 eV in **3**. The r.m.s. deviations between the geometrically optimized bond lengths, bond angles and the corresponding crystallographically determined values are 0.016 Å, 3.6° in **2**, and 0.022 Å, 3.1° in **3**.

The net charges of atoms and dipoles calculated at the BLYP level (Supplementary Table 2) indicate that all oxygen and nitrogen atoms in the molecules of **2** and **3** bear negative charges, and the sulfur atom (S1) of the methanesulfonamide group and the carbon atoms of the oxygen-bridged phenyl rings having substitutions (C3, C5, C6 and C7) bear positive charges; the remaining carbon atoms (except C14–C17 atoms in **3**) bear negative charges. Due to this charge redistribution, the dipole of the molecule becomes 2.84 a.u. for **2** and 2.81 a.u. for **3**, respectively.

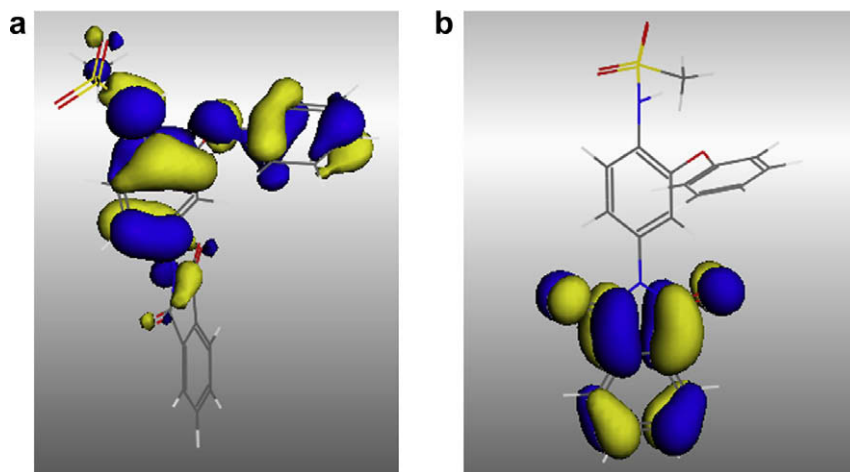


Fig. 5. Charge density of (a) HOMO and (b) LUMO orbitals of $C_{13}H_{14}O_3N_2S$ (**2**) calculated by DFT method.

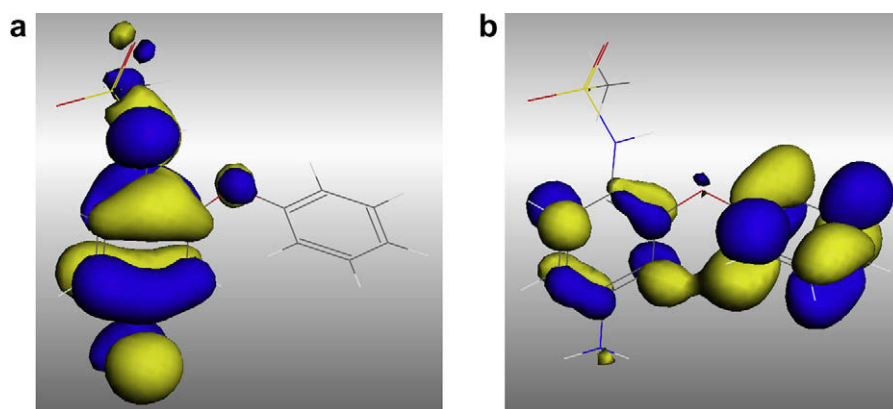


Fig. 6. Charge density of (a) HOMO and (b) LUMO orbitals of $C_{21}H_{16}O_5N_2S$ (**3**) calculated by DFT method.

The HOMO (highest occupied molecular orbital) and LUMO (lowest unoccupied molecular orbital) wave functions in molecules of **2** and **3** are quite different, and the charge densities for the HOMO and LUMO in **2** (Fig. 5) and **3** (Fig. 6) indicate very little charge accumulation on the hydrogen atoms. In **2**, the HOMO is primarily localized on the electron-rich amino and methanesulfonamide groups at the C3 and C6 positions of the phenyl ring A (C1–C6) as well as on the bridging oxygen atom (O1) with hardly any population on the phenyl ring B (C7–C12). In the HOMO of **2**, the benzene ring (A) atoms have equal contribution and show bonding–antibonding patterns characteristic of phenyl ring system. It is worth pointing out that the corresponding HOMO population in **3** is associated with both oxy-bridged phenyl rings A and B, the nitrogen (N1 and N2) and oxygen (O1) atoms. The LUMO in **2** is populated on the carbon atoms of phenyl rings A and B with only minor population localized on the bridging oxygen (O1) and amide nitrogen (N1) atoms. In **3**, however, the LUMO population is located mainly on the dioxo-1,3-dihydroisindol-2-yl part of the molecule with almost no charge accumulation on the phenoxyphenyl methanesulfonamide fragment.

The orbital energy level analysis at the BLYP level shows E_{HOMO} and E_{LUMO} values of -4.86 and -1.44 eV for **2**, and -5.52 and -3.31 eV for **3**, respectively. The HOMO–LUMO energy separation has been used as an indicator of kinetic stability of the molecule [35,36]. A large HOMO–LUMO gap implies a high kinetic stability and low chemical reactivity, because it is energetically unfavorable to add electrons to a high-lying LUMO or to extract electrons from

a low-lying HOMO [36]. In the present work, the HOMO–LUMO energy gap in **3** (2.21 eV) is found to be smaller than that in **2** (3.42 eV), which suggests that the compound **3** is likely to be more reactive than compound **2**. The differences between the orbital energies corresponding to HOMO–1 and HOMO–2 of 0.67 eV in **2** and 0.54 eV in **3** are much larger than 0.05 eV, which indicate that the HOMO–1 and HOMO–2 energy levels in compounds **2** and **3** are non-degenerate. Similar conclusion can be drawn from the LUMO+1 and LUMO+2 orbital energy calculations in **2** and **3**.

According to the molecular orbital theory, HOMO and LUMO are two important factors influencing the bioactivity of a compound. Preliminary results of anti-inflammatory activity test using the rat carrageenan paw edema model indicate that compound **3** can induce 34% edema inhibition in the rat paws, while compound **2** does not exhibit any anti-inflammatory activity; the corresponding edema inhibition with diclofenac sodium (reference drug) is 66%. The interaction between compound **3** and the receptor cells of inflamed tissue in animal models can be dominated by $\pi \dots \pi$ or hydrophobic interactions among the frontier orbitals. The negative charges in **3**, mainly located on the nitrogen and oxygen atoms of the sulfonamide and dioxoisindol-2-yl groups, are likely to interact with the positive part of the receptor. The most positively charged parts of **3**, on the contrary, will interact quite easily with the negatively charged part of the receptor. The anti-inflammatory activity of **3** can possibly be attributed to the presence of additional oxygen acceptor atoms in the dioxoisindol-2-yl part of the mole-

cule and the molecular conformation which facilitate $\pi \dots \pi$ stacking interaction.

4. Conclusions

Two nimesulide derivatives, N-(4-amino-2-phenoxyphenyl) methanesulfonamide (**2**) and N-[4-(1,3-dioxo-1,3-dihydroisindol-2-yl)-2-phenoxyphenyl] methanesulfonamide (**3**), were synthesized and their crystal structures have been solved using laboratory X-ray powder diffraction data. The molecular geometry and the electronic structure of **2** and **3** have been analyzed by the DFT calculations. The observed molecular conformations of the compounds as established by the X-ray analysis agree well with that obtained from the quantum mechanical calculations. Intermolecular N–H...O hydrogen bonds in **2** generate a two-dimensional supramolecular assembly of $R_4^4(12)$ and $R_4^4(36)$ rings, whereas in **3** a three-dimensional supramolecular framework is formed by a combination of N–H...O, C–H...O hydrogen bonds and $\pi \dots \pi$ stacking interactions. The HOMO–LUMO energy separation suggests that compound **3** is likely to be more reactive than compound **2**. The anti-inflammatory activity evaluated using the rat paw edema model indicates that compound **3** can induce 34% edema inhibition in rat paws, while the compound **2** does not exhibit any anti-inflammatory activity. The present study is promising for resolving the structure at an atomic resolution of pharmaceutical compounds that can not be easily obtained as single crystals suitable for conventional X-ray structure analysis.

Acknowledgements

Financial support from the University Grants Commission, New Delhi, and the Department of Science and Technology, Government of India, New Delhi, through the DRS (SAP-1) and FIST programs for purchasing the Bruker D8 Advance X-ray powder diffractometer, is gratefully acknowledged. AB thanks the University Grants Commission, India, for a research fellowship. We also thank Prof. Monika Mukherjee, IACS, Kolkata, for helping in DFT calculations.

Appendix A. Supplementary data

Crystallographic data for the structures $C_{13}H_{14}O_3N_2S$ (**2**) and $C_{21}H_{16}O_5N_2S$ (**3**) reported in this article have been deposited with the Cambridge Crystallographic Data Centre as supplementary publication numbers CCDC 761790 and 761791. Supplementary

data associated with this article can be found, in the online version, at doi:10.1016/j.cplett.2010.05.009.

References

- [1] D.E. Griswold, J.L. Adams, *Med. Res. Rev.* 16 (1996) 181.
- [2] G.F. Fabiola, V. Patabbi, K. Nagrajan, *Bioorg. Med. Chem.* 6 (1998) 2337.
- [3] A. Bennet, *Rheumatology* 38 (Suppl. 1) (1999) 1.
- [4] C. Michaux, C. Charlier, F. Julémont, X. de Leval, J. -M. Dogné, B. Pirotte, F. Durant, *Eur. J. Med. Chem.* 40 (2005) 1316.
- [5] T. Inaba, K. Tanaka, R. Takeno, H. Nagaki, C. Yoshida, S. Takano, *Chem. Pharm. Bull.* 48 (2000) 131.
- [6] F. Julémont et al., *J. Med. Chem.* 47 (2004) 6749.
- [7] R. García-Nieto, C. Pérez, F. Gago, *J. Comput.-Aided Mol. Des.* 14 (2000) 147.
- [8] R.G. Kurumbail et al., *Nature* 384 (1996) 644.
- [9] K.D.M. Harris, M. Tremayne, B.M. Kariuki, *Angew. Chem. Int. Ed.* 40 (2001) 1626.
- [10] W.I.F. David, K. Shankland, L.B. McCusker, C. Baerlocher (Eds.), *Structure Determination from Powder Diffraction Data*, OUP/IUCr, 2002.
- [11] S. Pagola, P.W. Stephens, D.S. Bohle, A.D. Kosar, S.K. Madsen, *Nature* 404 (2000) 307.
- [12] H. Nowell, J.P. Attfield, J.C. Cole, P.J. Cox, K. Shankland, S.J. Maginn, W.D.S. Motherwell, *New J. Chem.* 26 (2002) 469.
- [13] K.D.M. Harris, *Mater. Manuf. Processes* 24 (2009) 293.
- [14] W.I.F. David, K. Shankland, *Acta Cryst. A* 64 (2008) 52.
- [15] B. Chattopadhyay, S. Basu, P. Chakraborty, S.K. Choudhuri, A.K. Mukherjee, M. Mukherjee, *J. Mol. Struct.* 932 (2009) 90.
- [16] A. Altomare, C. Giacovazzo, A. Guagliardi, A.G.G. Moliterni, R. Rizzi, E. Werner, *J. Appl. Cryst.* 33 (2000) 1180.
- [17] A. Altomare et al., *J. Appl. Cryst.* 37 (2004) 1025.
- [18] M.M. Hall, V.G. Veeraraghavan, H. Rubin, P.G. Winchell, *J. Appl. Cryst.* 10 (1977) 66.
- [19] P.J.M. van Laarhoven, E.H.L. Aarts, *Simulated Annealing: Theory and Applications*, D. Riedel Publishing, Holland, 1987.
- [20] V.F. Nicolini, R. Cerny, *J. Appl. Cryst.* 35 (2002) 734.
- [21] J.J.P. Stewart, *MOPAC Version 5.0*, A General Purpose Molecular Orbital Package, QCEP, p. 455.
- [22] A.C. Larson, R.B.V. Dreele, *General Structure Analysis System (GSAS)*, Los Alamos National Laboratory Report, LA-UR 86-748G, 1994.
- [23] B.H. Toby, *J. Appl. Cryst.* 34 (2001) 210.
- [24] B. Delley, *J. Chem. Phys.* 92 (1990) 508.
- [25] J.P. Perdew, K. Burke, M. Ernzerhof, *Phys. Rev. Lett.* 77 (1996) 3865.
- [26] A.D. Becke, *Phys. Rev. A* 38 (1988) 3098.
- [27] A.C. Lee, W. Yang, R.G. Parr, *Phys. Rev. B* 37 (1988) 785.
- [28] C.A. Winter, E.A. Risley, R.H. Silber, *J. Pharmacol. Exp. Ther.* 162 (1968) 196.
- [29] L. Dupont, *Acta Cryst. C* 51 (1995) 507.
- [30] C. Michaux et al., *Acta Cryst. C.* (2002) 88.
- [31] P. Smith-Verdier, S. Garcia-Blanco, F. Florencio, *Acta Cryst. B* 32 (1976) 2006.
- [32] M. Szabo, D. Ban, C. Rat, A. Silvestru, J.E. Drake, M.B. Hursthouse, M.E. Light, *Inorg. Chem. Acta* 357 (2004) 3595.
- [33] B.T. Gowda, S. Forob, H. Fuess, *Acta Cryst. E* 63 (2007) o2570.
- [34] J. Bernstein, R.E. Davis, L. Shimoni, N.L. Chang, *Angew. Chem. Int. Ed. Engl.* 34 (1995) 1555.
- [35] K.H. Kim, Y.K. Han, J. Jung, *Theor. Chem. Acc.* 113 (2005) 233.
- [36] J. Aihara, *J. Phys. Chem. A* 103 (1999) 7487.